THE ASTROPHYSICAL JOURNAL, 371:36–48, 1991 April 10

HIGH-RESOLUTION SPECTROSCOPY OF Q1100−264 AGAIN

R. F. CARSWELL AND K. M. LANZETTA
Institute of Astronomy, Madingley Road, Cambridge CB3 0HA, UK

H. C. PARNELL
Department of Astrophysics, Oxford University, Nuclear Physics Building, Keble Road, Oxford OX1 3RH, UK

AND

J. K. WEBB
Royal Greenwich Observatory, Madingley Road, Cambridge CB3 0EZ, UK
Received 1990 July 5; accepted 1990 September 21

ABSTRACT

The results of echelle spectrometry with resolution $\lesssim 9$ km s^{-1} of the Lyα forest region of Q1100−264 are described. The Lyα forest systems show a range of Doppler parameters from 12 km s^{-1} to about 80 km s^{-1}, with rather large uncertainties for the low H I column density systems particularly. Few of these systems have low Doppler parameters, and there is no significant trend of Doppler parameter with H I column density, in contrast with the results of Pettini et al. from the study of a different quasar. The six heavy element systems with lines in the observed spectral region are all found to have complex velocity structure, on scales ranging from $\lesssim 10$ km s^{-1} to ~ 150 km s^{-1}.

Subject headings: cosmology — quasars

1. INTRODUCTION

There has been intense observational and theoretical interest in the properties of the absorption systems seen in QSO spectra, and their relation to galaxies and the intergalactic medium. The systems which show heavy elements have the potential for revealing abundances and clustering properties of material at high redshifts, and those for which only H I lines are seen may arise in proto-galaxies or material in the intergalactic medium. In either case the primary requirements for further analysis are the redshifts, Doppler widths and column densities for the ions seen in each cloud, and the reliable determination of these quantities involves obtaining spectra of high-redshift quasars at resolutions of order 10 km s^{-1} or better.

For the Lyα forest systems it is possible to determine the Doppler parameter and H I column density distribution for systems for which the component structure is adequately resolved. Estimates for the Doppler widths based on work at resolutions $\sim$20–30 km s^{-1} (FWHM) yield average $b = \sqrt{2}\,\sigma$ values of order 30 km s^{-1} (Carswell et al. 1984, from an earlier study of Q1100−264; Atwood, Baldwin, & Carswell 1985), corresponding to temperatures of order 5×10^4 K if they are thermal. Model calculations (e.g., Baron et al. 1989) lead to temperatures of $\sim 2 \times 10^4$ K, and size and ionization arguments lead to temperatures of $\sim 3 \times 10^4$ K or more (Chaffee et al. 1986). Thus the minimum Doppler width is of critical importance as a model discriminator, and observations at high resolution and relatively high signal-to-noise ratios (S/N) are required to establish this quantity.

Results of such observations have been published in two cases. Chaffee et al. (1983) obtained 12 km s^{-1} resolution spectra of PHL 957 in a small number of wavelength regions, and report one Lyα system with a Doppler parameter $12 \lesssim b \lesssim 17$ km s^{-1}, and so a cloud temperature $\lesssim$17,000 K. Results by Pettini et al. (1990) from 6 km s^{-1} resolution spectra place tighter constraints on the minimum Doppler parameters, and the temperatures of the clouds are in some cases below 5000–10,000 K for a sight line towards the quasar Q2206−199. These low temperatures are difficult to reconcile with any currently popular model.

For the heavy element systems it is of interest to obtain a sufficiently large sample of such systems at the highest possible resolution to see if there is component structure with widths on scales of 1 or 2 km s^{-1} corresponding to possible thermal broadening. By determining Doppler parameters for a number of heavy element lines with a range of atomic masses, e.g., from C^{12} to Fe^{56}, it may be possible to separate the thermal velocity widths from any component due to bulk motions using the fact that only the thermal widths depend on the atomic mass.

Here we present 9 km s^{-1} resolution echelle spectra of the bright $z_{em} = 2.14$ quasar Q1100−264, covering the region from a strong Lyα absorption at $z = 1.839$ to the Lyα emission line, and results from Voigt profile fits to all the observed features in this wavelength range.

2. OBSERVATIONS AND ANALYSIS

Spectra of Q1100−264 were obtained on the nights of 1990 January 31 and February 1 and 3 using the UCL echelle spectrograph at the Coudé focus of the Anglo Australian Telescope. The system is described by Walker & Diego (1985) and Walker et al. (1986). The instrument setup was very similar to that described by Pettini et al. (1990), with the only significant differences being that the wavelength range covered by the IPCS detector was 3434–3906 Å, and the slit width used here was 1".25. As with the Pettini et al. observations, the slit was maintained at the parallactic angle throughout the observations to minimize light losses through atmospheric refraction, and for wavelength calibration and determination of the instrument resolution exposures of a Th-Ar lamp were obtained every hour. The slit width was somewhat less than that of the seeing profile, and guiding was done off the spectrograph slit, so the resolution element is properly defined by the slit width and not the seeing profile of the object. Table 1 summarizes the integration times and observing conditions.

The data were extracted using a variant of the optimal tech-

TABLE 1

OBSERVATIONS

Start (UT)	Exposure (s)	Comments
1990 Feb 1.59..........	3600	
1.63..........	3600	Light cloud
1.68..........	3600	Light cloud
1.73..........	3600	
Feb 2.68..........	3600	Cloud clearing
2.73..........	3765	
Feb 4.60..........	3600	Mountain cloud
4.65..........	3600	all night
4.70..........	2426	

nique described by Robertson (1986), modified to allow for the fact that the echelle orders are not parallel. An array of variances was determined at the same time and retained for later use in assessing the reality of any features and the accuracy of the parameters determined from the absorption lines.

Th-Ar spectra were obtained before and after each object observation. These two wavelength comparison runs were extracted using the same spatial weights as were used for the object, and then summed after checking that no unacceptably large shifts had occurred. The wavelength scale was then determined for each object integration, and the individual object and comparison arcs were summed on to a uniform wavelength scale using weights chosen to maximize the S/N in the object spectrum. In fact the echelle system is so stable that this rebinning is not strictly necessary for a single night's observations, but after changing the spectrograph settings for different objects we could not guarantee returning to exactly the same wavelength calibration, so for the final summed data some rebinning was needed. In each order of the summed data the spectral resolution as a function of wavelength was determined by fitting quadratic polynomials in wavelength to the measured full width at half-maxima (FWHM) of the unblended Th-Ar lines. There was a small amount of variation with the wavelength, but the resolution is typically 8.5–9 km s^{-1} (FWHM).

First estimates of the continua were made for each order by using spline fits to spectral regions which are apparently line free, and deviations from this continuum in these regions were compared with the variance array to isolate any significantly low values. These were then removed and a new continuum estimate formed. This process was repeated until the scatter in the remaining continuum points was consistent with that expected on the basis of the variance estimates. The final spectra normalized by this continuum are shown in Figure 1.

An absorption line list was generated using the technique described by Young et al. (1979). The absorption lines selected have a probability of $\leq 10^{-5}$ of being due to chance against the fitted continuum. The heliocentric vacuum wavelengths and equivalent widths are given in Table 2. Where clear component structure was seen then the parameters for the components are given, but since these were found by seeking local maxima within a profile the results will not necessarily correspond to the components found by profile fitting. Similarly, the equivalent widths were determined by summing contributions from each pixel directly, and profile fitting may give somewhat different results.

For each significant feature Voigt profiles convolved with the instrument profile were fitted to derive the redshift z, Doppler parameter $b\,(=\sqrt{2}\,\sigma)$, and column density N for each component, with the best fit determined by minimizing χ^2. Oscillator strengths were taken from the compilation by Morton, York, & Jenkins (1988). The number of components assigned to any profile is the minimum number for which the χ^2 value has $>1\%$ probability of being due to chance. While this limit appears generous, in practise the addition of a single component almost invariably changed a very poor fit (probability <0.01) to a good one (probability ~ 0.5). A check was made (using a K-S test) after fitting all profiles that the probability distribution overall was consistent with a uniform one. For the Lyα forest systems only a single line is available in the observed range, but for some of the heavy element systems in this object there are a number of lines available. Under these circumstances we have fitted all lines simultaneously, allowing the column densities for differing ions to vary freely, but constraining the redshifts to be the same for all and imposing a relationship on the Doppler parameters. It is the Doppler parameter constraint which involves an element of choice, since the velocity widths for all ions could be roughly the same if bulk motions are the dominant cause, or inversely proportional to the square root of the atomic mass if the widths are thermal. In general we found that the bulk motion approximation provided marginally better fits, suggesting temperatures $\lesssim 10^4$ K. The results of the profile fits are contained in Table 2.

Note that because the data is rebinned the values in neighboring channels are not statistically independent. To allow for this we determined a χ^2 scale factor from continuum regions in the summed data, and applied this to the values obtained for the trial profile fits. Simulated data showed that this should give correct answers for the parameter values and (from the Hessian matrix) their error estimates. However, the correlation between neighbors in the rebinned data will depend on how the bins in the raw data map into the final sum, and this will usually depend on the position in the spectrum. Thus a χ^2 correction which we have derived on the basis of the global continuum properties may not apply accurately for an individual absorption feature, though on average χ^2/ν, the value normalized to the number of degrees of freedom, should be ~ 1. For our data $\langle \chi^2/\nu \rangle = 1.016 \pm 0.024$, so on average we have not significantly under- or overfitted the data. It is difficult to be as confident in individual cases, but we are unlikely to be badly wrong. When there are too few components fitted to a complex the χ^2 value tends to be very high, while as components are added to a complex which is adequately fitted with fewer there is a relatively slow reduction in the normalized χ^2 when the profiles are well oversampled as is usually the case here.

Comparison of the results obtained here with those of a previous study by Carswell et al. (1984) shows good general agreement in the line equivalent widths (allowing for the difficulties in setting the continuum level), and for the Lyα lines, the inferred velocity structure, H I column densities and Doppler parameters. More complex structure is found in the heavy element systems from the higher resolution spectra described here. There is a discrepancy in wavelengths, and hence redshifts, which is removed if we apply a heliocentric correction (-11.3 km s^{-1}) to their data.

3. Lyα SYSTEMS

As usual, most of the absorption lines shortward of the Lyα emission are likely to be Lyα in absorption, though we cannot

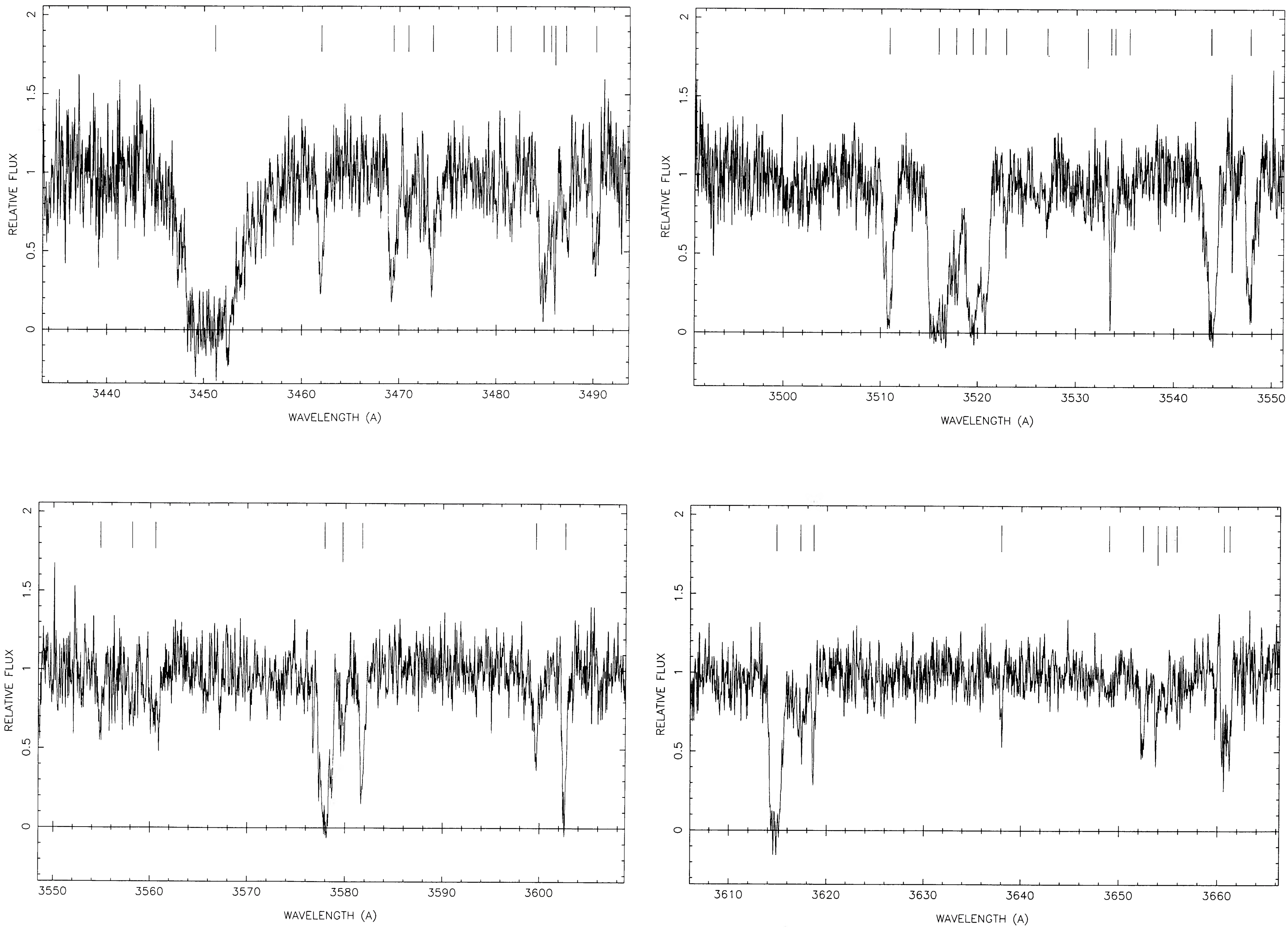

FIG. 1.—Echelle spectrum of Q1100−264, normalized to unit continuum. The data have been smoothed using a Gaussian filter with FWHM 0.02 Å for display purposes.

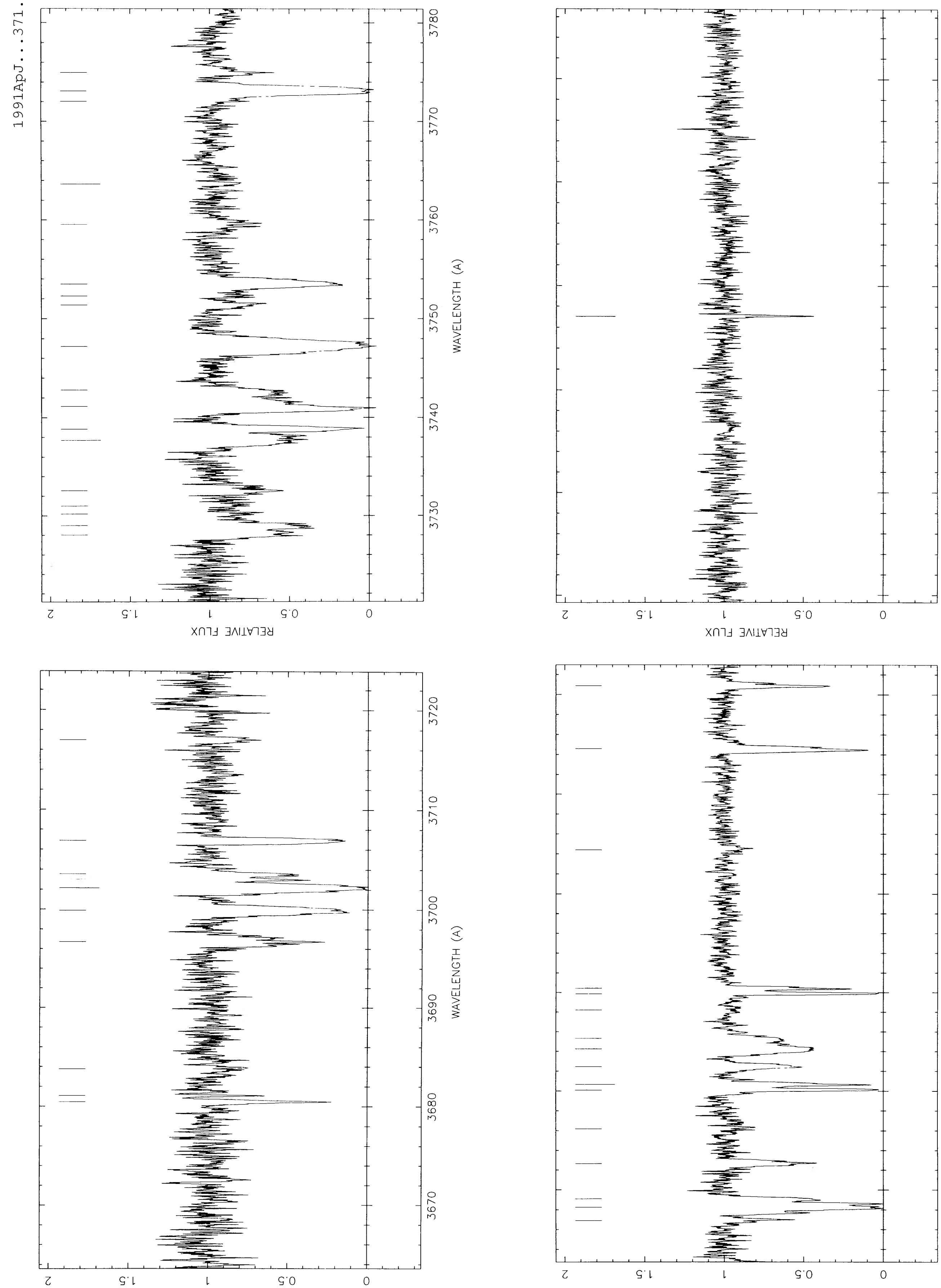

FIG. 1—*Continued*

TABLE 2

ABSORPTION LINES IN Q1100–264

n	λ_{vac}	±	EW_{obs}	±	χ^2/ν	ID	z	±	b	±	log N	±	σ_R	p	Comments
1..........	3451.15	0.078	7.197	0.163	0.875	Lyα	1.837720	...	6.0	...	18.278	...	0.043	0.996	
						Lyα	1.838237	...	13.9	...	18.532	...			
						Lyα	1.838557	...	10.8	...	18.778	...			
						Lyα	1.838732	...	7.1	...	18.689	...			
						Lyα	1.838914	...	6.8	...	18.762	...			
						Lyα	1.839201	...	14.9	...	18.622	...			
						Lyα	1.839372	...	0.8	...	17.158	...			
2..........	3461.97	0.051	0.459	0.053	0.605	Lyα	1.847767	0.000019	26.5	2.7	13.631	0.044	0.042	0.995	
3..........	3469.40	0.030	0.650	0.044	1.223	Lyα	1.853858	0.000028	37.4	3.8	13.819	0.045	0.045	0.044	
4..........	3470.92	0.057	0.217	0.039		Lyα	1.855129	0.000064	33.0	9.5	13.208	0.104			
5..........	3473.40	0.058	0.619	0.054	1.260	Lyα	1.857120	0.000034	38.4	4.7	13.672	0.050			
						Si IV λ1402	1.476725	0.000006	8.8	1.7	12.857	0.167			z and b tied to C IV at $T = 0$ K
6..........	3480.02	0.032	0.096	0.024	1.306	Lyα	1.862634	0.000041	14.7	6.6	12.921	0.143	0.052	0.011	
7..........	3481.44	0.067	0.185	0.039		Lyα	1.863835	0.000060	26.9	8.8	13.126	0.118			
8..........	3484.84	0.020	0.750	0.037	1.209	Lyα	1.866589	0.000069	36.6	6.5	13.896	0.113	0.057	0.037	noisy profile
9..........	3485.62	0.017	0.140	0.019		Lyα	1.867334	0.000268	47.6	29.1	13.491	0.254			
10..........	3486.04	0.024	0.237	0.030		Lyα	1.867592	0.000021	3.9	7.5	13.340	1.405			
11..........	3487.14	0.041	0.294	0.038		Lyα	1.868542	0.000048	32.4	7.5	13.369	0.081			
12..........	3490.23	0.047	0.371	0.055	0.801	Lyα	1.871007	0.000035	28.9	5.0	13.535	0.068	0.045	0.883	
13..........	3510.87	0.032	0.958	0.048	0.924	Lyα	1.887977	0.000019	41.3	2.5	14.047	0.033	0.045	0.679	two components??
14..........	3515.91	0.015	2.152	0.042	0.986	Lyα	1.891825	0.000036	38.9	4.2	14.510	0.101	0.046	0.555	
						Lyα	1.892652	0.000025	16.8	7.1	15.097	1.146			
15..........	3517.71	0.025	0.748	0.033		Lyα	1.893516	0.000052	62.1	9.5	14.013	0.050			
16..........	3519.41	0.013	1.349	0.034		Lyα	1.895085	0.000025	45.3	4.5	14.378	0.053			
17..........	3520.73	0.014	0.822	0.029		Lyα	1.896119	0.000026	35.0	3.3	14.023	0.043			
18..........	3522.85	0.037	0.131	0.025	1.352	Lyα	1.897889	0.000035	17.5	5.1	13.041	0.103	0.046	0.056	
19..........	3527.05	0.066	0.179	0.034	0.753	Lyα	1.901330	0.000040	28.4	5.8	13.127	0.075	0.047	0.903	
20..........	3531.18	0.073	0.210	0.037	1.179	Lyα	1.904725	0.000115	61.4	19.2	13.254	0.106	0.047	0.150	
21..........	3533.57	0.027	0.205	0.025	1.021	Fe II λ2600	0.358972	0.000002	4.6	0.8	14.029	0.478	0.048	0.533	tied to Mg II and Mg I $T = 1000$ K
22..........	3534.01	0.020	0.117	0.018		Fe II λ2600	0.359136	0.000001	5.9	0.5	12.946	0.097			tied to Mg II, $T = 1000$ K
23..........	3535.46	0.080	0.151	0.035	1.091	Lyα	1.908241	0.000096	43.5	14.2	13.070	0.119	0.048	0.283	
24..........	3543.72	0.021	1.197	0.042	0.818	Lyα	1.914520	0.000064	25.0	7.6	13.270	0.138	0.049	0.894	in two orders
						Lyα	1.915180	0.000021	30.3	3.0	14.262	0.075			parameters uncertain
25..........	3547.75	0.026	0.628	0.047	0.846	Lyα	1.918355	0.000024	31.8	3.1	13.849	0.050	0.048	0.834	
26..........	3554.87	0.050	0.189	0.037	0.687	Lyα	1.924185	0.000036	25.1	5.2	13.199	0.076	0.045	0.973	
27..........	3558.14	0.045	0.154	0.031	0.921	Lyα	1.926896	0.000063	34.4	9.2	13.130	0.099	0.044	0.775	
28..........	3560.55	0.065	0.320	0.044		Lyα	1.928871	0.000063	57.8	9.1	13.469	0.059			
29..........	3577.89	0.024	1.420	0.043	1.137	Si II λ1260	1.837720	0.000009	6.0	1.7	12.566	0.096	0.052	0.139	all tide to C II, O I at $T = 0$ K
						Si II λ1260	1.838237	0.000016	13.9	2.2	13.067	0.069			
						Si II λ1260	1.838557	0.000020	10.8	2.4	13.491	0.139			
						Si II λ1260	1.838732	0.000018	7.1	3.7	13.022	0.239			
						Si II λ1260	1.838914	0.000008	6.8	1.3	13.539	0.069			
						Si II λ1260	1.839201	0.000012	14.9	2.5	13.122	0.070			
						Si II λ1260	1.839372	0.000012	0.8	1.2	12.807	1.325			
30..........	3579.71	0.045	0.282	0.034	1.073	Lyα	1.944648	0.000036	34.6	5.2	13.372	0.056	0.045	0.331	
31..........	3581.70	0.019	0.455	0.028	0.894	Lyα	1.946292	0.000013	23.5	1.8	13.652	0.034	0.046	0.702	
32..........	3599.57	0.039	0.356	0.034	1.123	Lyα	1.961024	0.000034	38.5	4.6	13.522	0.046	0.055	0.226	uncertain—end order
33..........	3602.56	0.025	0.490	0.039	0.893	Lyα	1.963415	0.000014	17.6	2.0	13.801	0.070	0.048	0.669	
34..........	3614.85	0.018	1.441	0.038	1.039	Lyα	1.973507	0.000014	40.6	2.6	14.499	0.075	0.045	0.336	
35..........	3617.29	0.060	0.446	0.043		Lyα	1.975495	0.000075	79.0	11.7	13.627	0.052			
36..........	3618.63	0.028	0.203	0.026		Lyα	1.976647	0.000014	10.5	2.2	13.209	0.076			
37..........	3637.95	0.050	0.108	0.024	0.879	Lyα	1.992581	0.000019	11.7	3.0	12.914	0.080	0.045	0.688	
38..........	3648.94	0.104	0.125	0.031	0.861	Lyα	2.001583	0.000107	53.2	15.5	13.014	0.106	0.048	0.821	
39..........	3652.38	0.036	0.257	0.027	0.822	Lyα	2.004416	0.000016	17.7	2.3	13.274	0.045	0.049	0.722	

TABLE 2—*Continued*

n	λ_{vac}	±	EW_{obs}	±	χ^2/ν	ID	z	±	b	±	log N	±	σ_R	p	Comments
40..........	3653.86	0.045	0.210	0.027	0.674	Al II λ1670	1.186824	0.000008	4.1	3.1	12.136	0.123	0.050	0.966	
						Lyα	2.005751	0.000094	32.7	12.2	13.005	0.156			
41..........	3654.73	0.038	0.101	0.020		Al II λ1670	1.187499	0.000017	12.3	3.8	12.006	0.098			
42..........	3655.79	0.085	0.142	0.031	1.386	Lyα	2.007422	0.000171	71.7	29.1	13.172	0.134	0.051	0.017	Continuum uncertain
43..........	3660.58	0.028	0.260	0.033	0.954	Lyα	2.011145	0.000034	19.7	5.3	13.364	0.089	0.052	0.568	continuum and wavelengths
44..........	3661.15	0.024	0.226	0.029		Lyα	2.011626	0.000036	18.3	5.3	13.281	0.096			uncertain—end of order
45..........	3680.46	0.020	0.234	0.021	0.893	Al II λ1670	1.202843	0.000006	10.1	1.2	12.528	0.045	0.047	0.686	
46..........	3681.08	0.016	0.046	0.012		Al II λ1670	1.203204	0.000013	1.1	8.7	11.927	4.435			
47..........	3683.78	0.054	0.092	0.022	1.253	Lyα	2.030223	0.000147	61.3	23.0	13.049	0.131	0.047	0.071	
48..........	3696.73	0.028	0.565	0.029	1.137	O I λ1302	1.838237	0.000016	13.9	2.2	13.262	0.224	0.052	0.139	all tied to C II and Si II
						O I λ1302	1.838557	0.000020	10.8	2.4	13.760	0.144			at $T = 0$ K
						O I λ1302	1.838732	0.000018	7.1	3.7	13.822	0.146			
						O I λ1302	1.838914	0.000008	6.8	1.7	14.136	0.067			
						O I λ1302	1.839201	0.000012	14.9	2.5	13.996	0.069			
						O I λ1302	1.839372	0.000012	0.8	1.2	13.300	0.690			
49..........	3699.89	0.021	0.809	0.029	0.984	Lyα	2.043482	0.000011	33.6	1.5	13.937	0.023	0.49	0.521	
50..........	3702.15	0.010	0.907	0.021	1.137	Si II λ1304	1.837720	0.000009	6.0	1.7	12.566	0.096	0.052	0.139	all tied to C II and O I
						Si II λ1304	1.838237	0.000016	13.9	2.2	13.060	0.069			at $T = 0$ K
						Lyα	2.045334	0.000016	26.0	2.0	14.068	0.047	0.52	0.139	
						Si II λ1304	1.838557	0.000020	10.8	2.4	13.491	0.139			
51..........	3703.01	0.012	0.177	0.014		Si II λ1304	1.838732	0.000018	7.1	3.7	13.022	0.239			
						Si II λ1304	1.838914	0.000008	6.8	1.3	13.539	0.069			
52..........	3703.56	0.022	0.272	0.021		Si II λ1304	1.839201	0.000012	14.9	2.5	13.122	0.070			
						Lyα	2.046476	0.000026	21.2	3.7	13.233	0.067			
						Si II λ1304	1.839372	0.000012	0.8	1.2	12.807	1.325			
53..........	3706.88	0.012	0.520	0.020	1.404	Lyα	2.049252	0.000010	20.9	1.4	13.802	0.034	0.51	0.021	
54..........	3716.99	0.032	0.134	0.019	0.925	Lyα	2.057576	0.000029	20.7	4.2	12.984	0.069	0.056	0.644	
55..........	3728.04	0.019	0.343	0.023	0.936	Lyα	2.066650	0.000046	28.6	5.2	13.401	0.093	0.047	0.748	
56..........	3729.00	0.022	0.553	0.027		Lyα	2.067356	0.000039	38.2	6.0	13.673	0.057			
57..........	3730.17	0.043	0.109	0.021		Lyα	2.068370	0.000069	32.5	12.3	13.022	0.128			
58..........	3731.00	0.060	0.112	0.023		Lyα	2.069234	0.000074	33.4	11.8	12.977	0.121			
59..........	3732.58	0.028	0.298	0.024		Lyα	2.070390	0.000034	41.6	4.9	13.404	0.043			
60..........	3737.69	0.019	0.623	0.024	1.141	Lyα	2.074674	0.000033	55.0	4.8	13.790	0.030	0.047	0.144	
61..........	3738.83	0.011	0.606	0.020		Lyα	2.075551	0.000010	20.3	1.4	13.805	0.036			
62..........	3741.14	0.013	1.019	0.024	0.836	Lyα	2.077207	0.000017	21.1	1.7	13.956	0.060	0.047	0.909	
63..........	3742.29	0.012	0.176	0.013		Lyα	2.077747	0.000070	37.4	15.9	13.528	0.186			
64..........	3742.80	0.036	0.222	0.023		Lyα	2.078564	0.000073	40.7	7.3	13.509	0.091			
65..........	3747.21	0.015	1.480	0.027	1.118	Lyα	2.082448	0.000011	49.2	1.4	14.301	0.020	0.047	0.168	
66..........	3751.36	0.039	0.184	0.021	0.931	Lyα	2.085834	0.000028	27.3	4.2	13.102	0.054	0.047	0.720	
67..........	3752.28	0.032	0.084	0.014		Lyα	2.086640	0.000038	23.7	5.9	12.892	0.084			
68..........	3753.48	0.015	0.825	0.022		Lyα	2.087594	0.000010	36.5	1.4	13.895	0.016			
69..........	3759.55	0.052	0.231	0.024	1.084	Lyα	2.092570	0.000046	47.5	6.4	13.216	0.050	0.048	0.268	
70..........	3763.64	0.041	0.067	0.014	1.151	Lyα	2.095960	0.000032	14.6	4.7	12.653	0.104	0.048	0.146	
71..........	3772.03	0.031	0.056	0.011	0.729	Lyα	2.102919	0.000052	28.5	7.6	12.856	0.095	0.094	0.991	
72..........	3773.10	0.008	1.083	0.017		Lyα	2.103736	0.000006	28.9	1.0	14.297	0.030			
73..........	3774.98	0.043	0.189	0.020	1.055	Lyα	2.105225	0.000026	27.7	3.5	13.100	0.046	0.050	0.361	
			Gap in coverage 3780–3883 Å												
74..........	3786.90	0.040	0.142	0.020	1.137	C II λ1334	1.837720	0.000009	6.0	1.7	13.351	0.072	0.052	0.139	all tied $T = 0$ K
75..........	3788.26	0.010	0.982	0.019		C II λ1334	1.838237	0.000016	13.9	2.2	13.658	0.064			
						C II λ1334	1.838557	0.000020	10.8	2.4	14.250	0.106			
						C II λ1334	1.838732	0.000018	7.1	3.7	13.901	0.182			
						C II λ1334	1.838914	0.000008	6.8	1.3	14.291	0.139			
76..........	3789.11	0.012	0.203	0.013		C II λ1334	1.839201	0.000012	14.9	2.5	13.808	0.056			
						C II λ1334	1.839372	0.000012	0.8	1.2	14.162	3.552			

TABLE 2—*Continued*

n	λ_{vac}	±	EW_{obs}	±	χ^2/ν	ID	z	±	b	±	log N	±	σ_R	p	Comments
77..........	3792.66	0.029	0.321	0.021	1.036	Mg II λ2796	0.356161	0.000111	19.5	24.6	12.153	0.692	0.046	0.386	
						Mg II λ2796	0.356228	0.000011	4.5	5.8	12.175	0.466			
						Mg II λ2796	0.356280	0.000007	0.9	3.7	13.791	11.144			
						Mg II λ2796	0.356320	0.000005	1.4	1.8	13.005	1.774			
						Mg II λ2796	0.356368	0.000005	0.8	3.1	13.567	9.097			
						Mg II λ2796	0.356413	0.000005	0.7	4.4	13.285	14.476			
78..........	3796.20	0.043	0.056	0.013	0.964	Lyα	2.122885	0.000097	52.4	13.6	12.875	0.093	0.048	0.566	
79..........	3800.10	0.008	0.350	0.011	1.021	Mg II λ2796	0.358825	0.000004	0.7	0.6	12.331	0.791	0.047	0.533	
						Mg II λ2796	0.358950	0.000010	5.2	0.8	13.549	0.659			
						Mg II λ2796	0.358972	0.000002	4.6	0.8	14.312	0.537			
80..........	3800.68	0.008	0.349	0.011		Mg II λ2796	0.359059	0.000004	1.0	0.5	12.437	0.375			
						Mg II λ2796	0.359136	0.000001	5.9	0.5	13.106	0.033			
						Mg II λ2796	0.359211	0.000002	2.3	0.6	12.592	0.110			
						Mg II λ2796	0.359316	0.000007	2.3	4.7	11.638	0.125			
81..........	3802.44	0.022	0.288	0.016	1.036	Mg II λ2803	0.356803	0.000111	19.5	24.6	12.153	0.692	0.046	0.386	
						Mg II λ2803	0.356228	0.000011	4.5	5.8	12.175	0.466			
						Mg II λ2803	0.356280	0.000007	0.9	3.7	13.791	11.144			
						Mg II λ2803	0.356320	0.000005	1.4	1.8	13.005	1.774			
						Mg II λ2803	0.356368	0.000005	0.8	3.1	13.567	9.097			
						Mg II λ2803	0.356413	0.000005	0.7	4.4	13.285	14.476			
82..........	3804.27	0.013	0.595	0.015	0.995	Lyα	2.129286	0.000022	35.7	2.4	13.596	0.034	0.046	0.499	
83..........	3805.31	0.015	0.219	0.011		Lyα	2.130085	0.000045	42.6	5.2	13.393	0.054			
84..........	3808.19	0.067	0.053	0.012	0.701	Lyα	2.132569	0.000068	34.3	9.6	12.559	0.100	0.045	0.959	
85..........	3809.87	0.008	0.336	0.010	1.021	Mg II λ2803	0.358825	0.000004	0.7	0.6	12.331	0.791	0.047	0.533	
						Mg II λ2803	0.358950	0.000010	5.2	0.8	13.549	0.659			
						Mg II λ2803	0.358972	0.000002	4.6	0.8	14.312	0.537			
86..........	3810.44	0.016	0.261	0.012		Mg II λ2803	0.359059	0.000004	1.0	0.5	12.437	0.375			
						Mg II λ2803	0.359136	0.000001	5.9	0.5	13.106	0.033			
						Mg II λ2803	0.359211	0.000002	2.3	0.6	12.592	0.110			
						Mg II λ2803	0.359316	0.000007	2.3	4.7	11.638	0.125			
87..........	3824.40	0.054	0.080	0.012	1.141	Lyα	2.145984	0.000047	30.7	6.5	12.717	0.076	0.046	0.194	
88..........	3834.58	0.010	0.505	0.013	1.260	C IV λ1548	1.476576	0.000028	6.3	3.5	12.872	0.262	0.050	0.016	
						C IV λ1548	1.476725	0.000006	8.8	1.7	13.769	0.046			
						C IV λ1548	1.476915	0.000012	9.5	2.0	13.295	0.068			
89..........	3840.89	0.023	0.291	0.015	1.260	C IV λ1550	1.476576	0.000028	6.3	3.5	12.872	0.262	0.050	0.016	
						C IV λ1550	1.476725	0.000006	8.8	1.7	13.769	0.046			
						C IV λ1550	1.476915	0.000012	9.5	2.0	13.295	0.068			
			Gap in coverage 3845–3849 Å												
90..........	3877.02	0.028	0.107	0.014	1.021	Mg I λ2852	0.358972	0.000002	4.6	0.8	11.930	0.049	0.048	0.533	tied to Mg II and Fe II, $T = 1000$ K

NOTE.—The quantity χ^2/ν is the normalized χ^2 value for the entire profile fitted, the instrument profile is fitted locally by a Gaussian with $\sigma = \sigma_R$ (Å), and p is the chance probability of the computed χ^2 value for the fit.

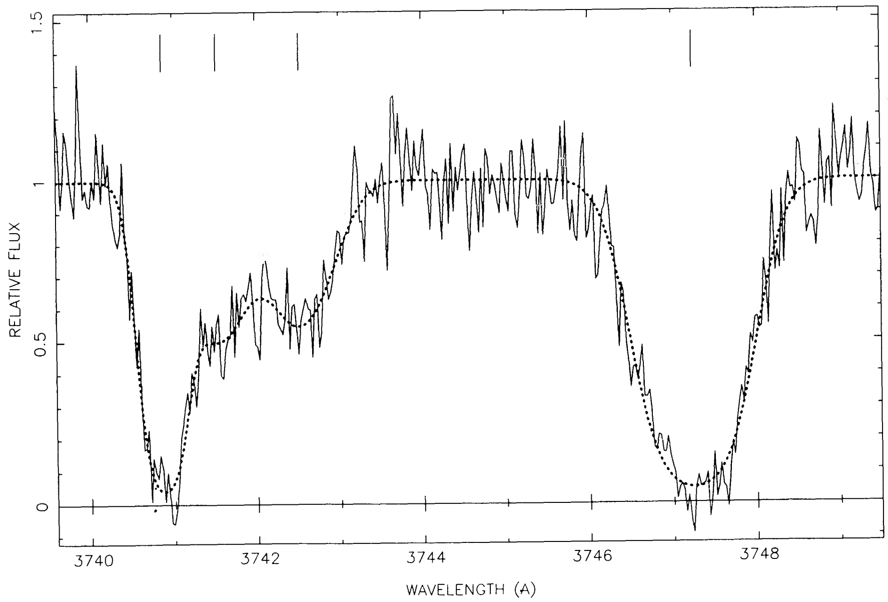

FIG. 2.—Region of the spectrum of Q1100−264 showing the raw data (*solid*) and fitted Voigt profiles convolved with the instrument profile (*dots*) for Lyα lines at $z = 2.077207, 2.077747, 2.078564$, and 2.082448. The tick marks indicate the line centers.

be absolutely sure that any individual line must be Lyα without some further information such as the presence of higher order Lyman lines at the same redshift. Examples of the Lyα profile fits are shown in Figure 2.

There are 71 Lyα lines in the redshift range $z = 1.84$ to 2.15, with a total H I column density per unit redshift of $10^{16.2}$ cm^{-2} at mean redshift $\langle z \rangle = 1.99$. This total column density should not be taken too seriously, since it is dominated by a single system at $10^{15.1 \pm 1.1}$ cm^{-2}, but the more reliable determinations [the 50 systems with log N(H I) error ≤ 0.1] yield a total column density per unit redshift of $10^{16.0}$ cm^{-2}. This figure probably provides a realistic lower limit. The data sample is limited, but the column density probability distribution for log N (H I) > 13.0 is consistent with a power law $dp(N) \propto N^{-\beta} dN$ where $\beta = 1.7 \pm 0.1$.

The mean Doppler parameter is $\langle b \rangle = 34$ km s^{-1}, similar to that found by Carswell et al. (1984), but the main difference between the results here and the earlier work is that the higher S/N and resolution results in much more precise determinations of this parameter for each line. The quantity $\sqrt{\langle (b - \langle b \rangle)^2/\sigma_b^2 \rangle} = 3.4$, where σ_b is the error estimate for b, so the spread in b-values of ± 14 km s^{-1} (1 σ) is mostly intrinsic rather than due to measurement errors. As a result we find that there are a few Lyα systems where the Doppler parameters are significantly less than 18 km s^{-1}. Thus at least those clouds must be cooler than the 2×10^4 K found in the Baron et al. (1990) model calculations. However, of the nine systems with $b < 18$ km s^{-1}, there are only three which are more than 1 σ below this value. One of these, at $z = 1.867592$ arises in a messy region centered on 3486 Å, with $b = 3.9 \pm 7.5$. The two narrow lines which are relatively clear are at 3618.62 Å and 3637.99 Å, corresponding to redshifted Lyα at $z = 1.976647$ and 1.992581. These have Doppler parameters 10.5 ± 2.2 and 11.7 ± 3.0, respectively. The lower redshift one is over 3 σ below 18 km s^{-1}, so, if it is a Lyα line, it must arise in a cool cloud.

However, we must verify that the few narrow candidate Lyα lines are not in fact heavy element lines. They are certainly not known lines from the list by Morton et al. (1988) in the known redshift systems listed here. It is tempting to ask if the line pair is a doublet, since the inferred column densities assuming they are due to H I are in the ratio 2:1, the Doppler parameters are similar, and they both occur in the same region of the spectrum. However the wavelength ratio would have to be 1.005353, which does not correspond to anything we are aware of. Candidate identifications with heavy element transitions fail because other expected lines are not seen in either our spectra or those published by Petitjean & Bergeron (1990), so there is no evidence to support the notion that these could be heavy element lines.

A further point which may be investigated is the correlation between the Doppler parameter b and the H I column density. Figure 3 shows all the Lyα systems we have found, apart from those associated with the $z = 1.839$ heavy element system, in the b–log N plane. There is little sign of a correlation between b and log N; the correlation coefficient is 0.11, and the probability that this value will be exceeded with uncorrelated data is 0.37.

However, the Doppler parameters are particularly uncertain at low column densities, and the values derived tend to depend on how one establishes the full-width zero intensity of a line. In general we have chosen to include a reasonable amount of continuum an either side of the line center in the profile fits, and this results in most cases in a broad rather than a narrow fitted line. Line 70 (Lyα at $z = 2.095960$) looks sharper than most of the weak features in the data, and has a best fit $b = 15 \pm 5$ km s^{-1} and log $N = 12.65 \pm 0.10$. However, even here an acceptable fit was obtained with a Doppler parameter $b = 70 \pm 20$ km s^{-1} and log $N = 12.99 \pm 0.11$ simply by choosing a slightly larger wavelength range to fit over. This sort of uncertainty affects many of the lines with $b \gtrsim 30$ km s^{-1} and log $N \lesssim 13.2$. Unfortunately we know of no way of compensating for this uncertainty, other than by obtaining better S/N data.

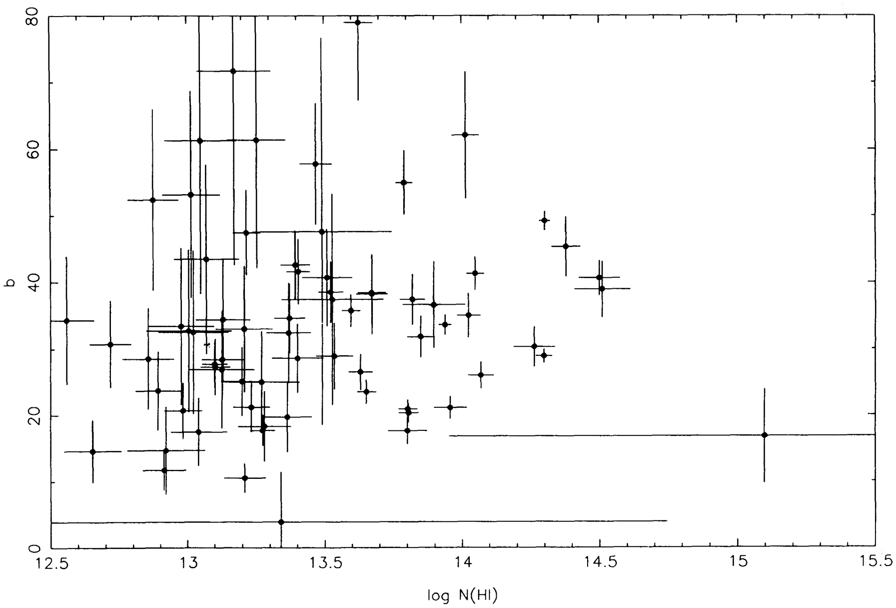

FIG. 3.—Doppler parameter b vs. log N(H I) for the Lyα forest systems at $z = 0.010$–9.990. The error bars at each point are 1 σ estimates.

If we try to allow for this uncertainty by excluding systems with log $N < 13.0$ and $\sigma_b > 0.25b$, then 43 Lyα lines remain in the sample and give a correlation coefficient 0.22, with a chance probability of 0.16. Thus there is no real case for a b–log N correlation even for the subsample, even though the σ_b restriction has the potential for introducing a spurious one.

Our Doppler parameter distribution and results of searching for a correlation between b and N seem to contrast with those of Pettini et al. (1990), who find several Lyα systems have $b < 18$ km s^{-1} and who find a strong correlation between b and log N. The two objects were observed with the same instrument, and the spectra have roughly the same resolution and S/N ratio, so we cannot appeal to instrumental differences as an explanation for the different results. Since they chose not to fit saturated or badly blended lines because of the uncertainties in the results, their column density upper limit will be a little lower than $N(\text{H I}) \sim 10^{14}$ cm^{-2}, so it is not surprising that they do not have as large a range of log N as we have found. It is not clear why they should find few high b–low log N systems if they are present (or we so many if they are generally absent), though some differences may arise because of selection and fitting procedures.

Because Pettini et al. (1990) fitted Voigt profiles to only a selected subset of their Lyα lines, it is difficult to compare the results directly. If we take their total sample to be the 89 lines which are not identified with heavy elements and restrict ourselves to the low b lines, then we can make some comparisons. For example, we find that nine of the 71 Lyα systems towards Q1100−264 have $b < 18$ km s^{-1} (corresponding to a temperature of 20,000 K for thermal broadening), while towards 2206−199 the number is 21 out of 89, a difference at only about the 10% significance level. For $b < 13$ km s^{-1} the numbers are 3/71 and 15/89, respectively, with significance level a little over 1%. In fact if we choose to exclude blended features because of the uncertainties, as was done by Pettini et al. (1990), then there are only two such narrow lines, and the two samples are different at the 0.5% level. Thus it is very likely that there is an excess of low b systems toward 2206−199 compared with Q1100−264 (though the different line selection criteria for the two objects make us slightly wary of advancing this claim strongly), and so we conclude that either the paths to the two quasars have Lyα clouds with somewhat different characteristics, or that there are a number of unidentified heavy element lines in the spectrum of 2206−199.

It is hard to defend this second possibility on the available data, as Pettini et al. (1990) point out. However, 2206−199 is unusual in that it has two damped Lyα systems, and while one, at $z = 2.076$ has apparently low heavy element abundances (Rauch *et al.* 1990), the other, at $z = 1.9203$, has strong heavy element lines. Indeed, the $z = 1.9203$ system is unusual in that Si II 1808, which has an oscillator strength $f = 0.0055$, is detected (Bergeron & Petitjean 1990). Thus it is possible that elements with abundances $\sim 10^{-3}$ that of silicon will be detectable in this system, so we have searched the available line lists for lines of neutral and singly ionized F, Ne, Na, P, Cl, Ar, K, Ca, Ti, Cr, Mn, Co and Ni, as well as the more usual ones at that redshift, but found no reasonable identifications. It is also notable at $z = 1.9203$ none of the Pettini et al. (1990) narrow features correspond to lines found in ζ Oph (Morton 1975) or ζ Pup (Morton 1978), so the Lyα identifications remain the most plausible possibility.

There are two observational tests which could confirm the Lyα identification for these narrow lines. One is to obtain high S/N spectra of 2206−199 in the Lyβ region and beyond. The Lyβ lines will be weaker, since the oscillator strength is about $\frac{1}{5}$ that of Lyα, but in the stronger narrow systems it should be detectable. An alternative approach is to observe the wavelength region just longward of the Lyα emission in the expectation that the unidentified heavy element line density, if that is the cause, will not change very much over such a short wavelength range, and so a number of unidentified heavy element lines would be found.

The redshift ranges for the Lyα lines in the two studies has a very small overlap ($1.845 \le z \le 2.105$ for Q1100−264, $2.087 \le z \le 2.587$ for 2206−199), so it is just conceivable that there is an extremely strong redshift dependence in the widths of the weak lines. However, until further objects observed and analyzed to determine the general pattern for the Lyα line widths we have no idea if extreme redshift dependence is needed, or which sight line should be regarded as typical, so we hesitate to draw conclusions about different conditions in Lyα clouds over quite large redshift ranges towards the two quasars. Despite this, we have no doubt that the possibilities will provide endless entertainment for others in the meantime.

4. HEAVY ELEMENT ABSORPTION SYSTEMS

4.1. *Individual Systems*

A number of heavy element redshift systems are known (Carswell et al. 1982, 1984; Petitjean & Bergeron 1990), and the data described here revealed no new ones. However the higher spectral resolution did reveal more complex velocity structure in a number of the known systems. Details are given for each complex below:

$z = 0.356$. The lines at 3792.68 and 3802.44 Å are identified with Mg II λ2796.352 and 2803.531. The equivalent width ratio is 1.09, so on a simple curve-of-growth analysis it is clear that the line centers should be optically thick. However, even at the resolution of these spectra (FWHM = 0.11 Å in this region), the residual intensity at the minimum is about half of the continuum intensity, so there must be several unresolved optically thick components in the line. The short-wavelength wing of the Mg II λ2803 profile is shallower than that for Mg II λ2796, while in the longer wavelength portions the depths of the two lines are comparable. This suggests that the short-wavelength components are likely to be optically thin, while there must be a number of higher redshift components which are optically thick. The decomposition of the profile into six components with redshifts from $z = 0.356160$ to 0.356413, with Doppler parameters ranging from 0.65 to 19.5 km s^{-1}, is given in Table 2 and shown in Figure 4. This decomposition is not unique, of course, but is a minimum component model which is consistent with the data.

Unfortunately there are no other lines in the observed wavelength region to check on the velocity structure. Fe II 2600 may be partly blended with a broad weak Lyα at 3527 Å, but there are no sharp features in this region, and the broad feature is at a wavelength larger than that expected for a Fe II blend. Neither Fe II λ2586 nor Mg I λ2582 are detected.

This system provides an example where a curve-of-growth analysis could be misleading. If the same data were to be obtained at 200 km s^{-1} resolution then the inferred single component column density for Mg II is $\log N = 13.4$, with a Doppler parameter of 8 km s^{-1}, while the total column density for the decomposition of the blend we have used is $\log N = 14.1$. Thus the Mg II column density derived on the assumption of a single system could be an underestimate by a factor of ~ 5.

$z = 0.359$. A galaxy has been found at this redshift 12″ from the quasar, corresponding to a distance of 50 kpc (for $H_0 = 100$ km s^{-1} Mpc^{-1}) at the distance of the galaxy (Bergeron & Boissé 1991, in preparation, reported by Petitjean & Bergeron 1990). The Mg II lines in this system were found to be split into two components by Carswell et al. (1984), and with the improved resolution and signal-to-noise ratio of the data here we find seven components with Doppler parameters in the range ~ 1–6 km s^{-1} spread in velocity over about 110 km s^{-1}. The total Mg II column density in this system inferred from these data is an uncertain $10^{14.42}$ cm^{-2}, compared with the value $10^{13.56}$ cm^{-2} inferred by Carswell et al. (1984). This serves to further highlight a point which is already widely

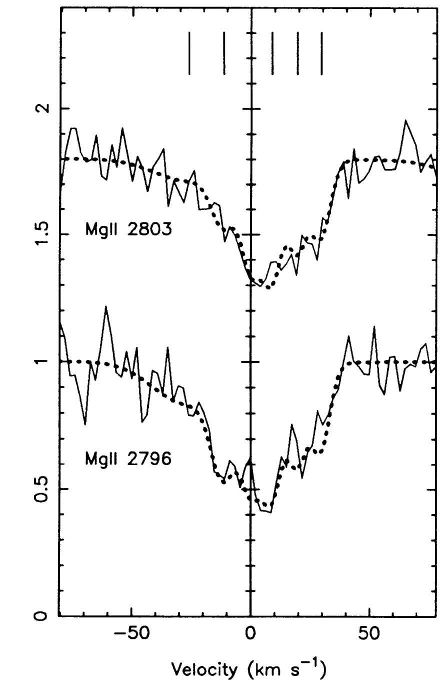

FIG. 4.—Mg II λ2796 and 2803 lines (*solid*) and fitted profiles (*dots*) on a velocity scale relative to the system at $z = 0.35628$. The other components in the complex are at velocities indicated by the tick marks. Each component has been normalized to unit continuum intensity, and a bias added to separate the different lines. Thus the zero level is one unit below the continuum for each individual line.

known but often ignored, that unresolved velocity structure gives an additional unquantified uncertainty in the column densities. Here the effect is about one order of magnitude, and there is, of course, no guarantee that the spectral resolution used here is high enough to yield the correct values.

Mg I λ2852 and Fe II λ2600 are both present in the $z = 0.358972$ component, and a weak Fe II λ2600 component is seen at $z = 0.359136$. We have chosen to derive column densities for these ions by assuming that the cloud temperatures are 10^3 K, corresponding roughly to the minimum Doppler parameter for a Mg II component seen is this system, with the rest of the velocity width arising from bulk motion. We could instead have assumed that bulk motion accounts almost entirely for the line widths, in which case the Fe II column density will be slightly smaller, or wholly thermal, where the column density will be slightly larger to compensate for its lower Doppler parameter (by a factor of $\sqrt{24/56} = 0.65$ from the mass ratio). Since only a single narrow Fe II component is seen in each case, we cannot differentiate between any of these possibilities.

The line profiles for this complex are shown in Figure 5.

$z = 1.187$. This system was found by Petitjean & Bergeron (1990) to have two Mg II components at $z = 1.18691$ and $z = 1.18746$, and they also detect Fe II at the lower redshift. We find Al II λ1670 in both components, at $z = 1.186824 \pm 0.000008$ and $z = 1.187449 \pm 0.000017$.

$z = 1.203$. This complex was discovered by Petitjean & Bergeron (1990), who reported Mg II components at $z = 1.20231$, 1.20284, and 1.20324, with the highest Mg II column density in the middle component. Only Fe II λ1608 and Al II λ1670 fall in the observed range here. The Fe II line is blended with a strong Lyα feature near the end of a spectral

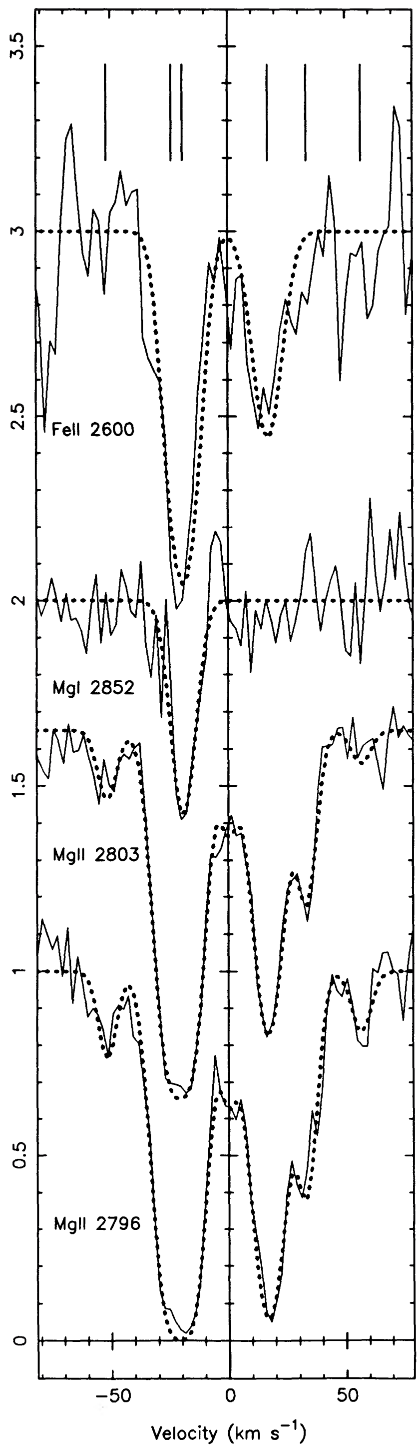

FIG. 5.—Mg II, Mg I, and Fe II lines in the $z = 0.359$ complex, shown on a velocity scale relative to the $z = 0.359059$ component. Other details are as for Fig. 4.

order and is consequently not measurable if it is present. The Al II line is found to have component structure, with a strong component at $z = 1.202843$ and a weak one at $z = 1.203204$.

z = 1.268. Petitjean & Bergeron (1990) found a weak Mg II doublet at redshift $z = 1.26771$. Al II λ1670 in this system lies in the C II λ1334 complex at $z = 1.839$, so is not detected, and there is no sign of Fe II λ1608 at 3467.5 Å.

z = 1.476. A C IV double was noted at this redshift by Carswell et al. (1982). There is clear component structure in the C IV lines here, with three components seen. The Si II λ1526 line would fall in a gap in the spectral coverage, but Si IV λ1393 and 1402 fall in the shortest wavelength region. The λ1393 line is lost in the damped Lyα line at 3450 Å, but there is a sharp feature corresponding to Si IV λ1402 at 3474.28 Å. The column density for Si IV in this system has been derived assuming that the $b = 8.8$ km s^{-1} found for C IV applies also for Si IV. The C IV λ1548, 1550, and Si IV λ1402 line profiles are shown in Figure 6.

z = 1.839. The C II λ1334, O I λ1302, and Si II λ1260, 1304, and 1526 lines were found by Carswell et al. (1984) to belong to a system with five velocity components with redshifts $z = 1.83786$ to 1.83938. Our analysis of the line profiles here reveals seven components with redshifts $z = 1.837720$ to 1.839372. These are shown in Figure 7. In this case the total column densities over the complex are in reasonable agreement with the earlier estimates; the C II column density is $10^{14.86}$ cm^{-2} (see $10^{14.79}$ by Carswell et al. 1984), O I λ$10^{14.60}$($10^{14.66}$), and Si II λ$10^{14.05}$($10^{14.21}$). Each of the components will have an associated Lyα making up the damped profile at 3450 Å. We have fitted this profile by fixing the redshifts for each of the component Lyα lines and allowing the H I column densities and Doppler parameters to vary to find a best fit. This results in huge (and unrealistic) error estimates for column densities for the individual components, but the best-fit total H I column density should be reasonably reliable. The individual results are given in Table 2, and the summed H I column density is $10^{19.42}$ cm^{-2}. If it is assumed that the Lyα line is single, then the best fit redshift is $z = 1.83857$ and H I column density $10^{19.40}$ cm^{-2}. The redshift is close to the $z = 1.838557$ found

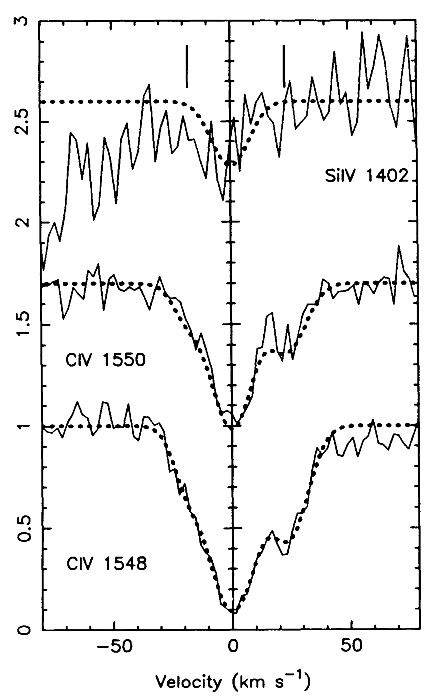

FIG. 6.—C IV and Si IV lines in the $z = 1.476$ complex, relative to the component at $z = 1.476725$. The Lyα lines blended with Si IV λ1402 have not been included in model profile, though they were used in determining the parameters for the line. Other details are as for Fig. 4.

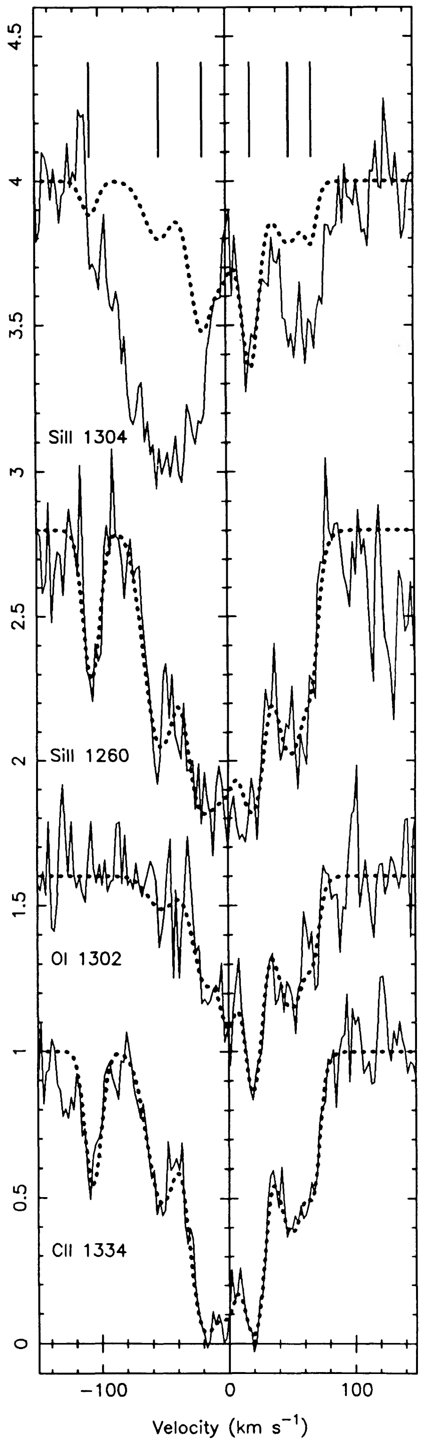

FIG. 7.—C II, O I, and Si II λλ1260, 1304 lines in the $z = 1.838$ complex, relative to the component at $z = 1.838732$. The Lyα lines blended with Si II λ1304 have been omitted from the displayed model profile, though they were included in the fitting procedure when the line parameters were determined. Other details are as for Fig. 4.

for one of the heavy element components, so it may be that this single cloud dominates the Lyα profile.

We cannot reliably convert these column densities to relative abundances because the H I column density is sufficiently low that ionization corrections can be important, a point noted in another context by Steigman, Strittmatter, & Williams (1975). If, despite this, we wish to interpret ion ratios as abundance ratios, then [Si/H] ~ -1.0, [C/H] ~ -1.2, and [O/H] ~ -1.7, so the complex may have abundances of order 1/10 solar. We have attempted to model the total column densities using the photoionization program CLOUDY (Ferland 1989), rather than for each component since the component-to-component shielding of any ionizing radiation will add to the uncertainties, and we do not really know what the H I column density is in each component. We find that a consistent photoionization model using an integrated quasar background spectrum gives the total column densities listed above, and N(C IV) $= 10^{14.21}$ from Carswell et al. (1984), with an ionization parameter log $U = -2.9$ and heavy element abundances $10^{-0.7}$ solar.

4.2. *General Properties of the Heavy Element Systems*

The five heavy element systems which show lines in our observed wavelength range show complex velocity structure. For four of these systems earlier investigations had revealed at least some of this structure; we have not added to the velocity information on the $z = 1.187$ and 1.203 systems known from the work of Petitjean & Bergeron (1990), but have found six components to a Mg II system at $z = 0.356$ where previously only two had been suspected from quite high-resolution data (Carswell et al. 1984), and seven at $z = 0.359$ where two were found previously. The system at $z = 1.476$ has three components in C IV. The velocity splittings within the complexes are less than about 200 km s^{-1} in all cases, apart from the 600 km s^{-1} separation between the Mg II complexes at $z = 0.356$ and 0.359. Thus the velocities are more typical of separations for gas clouds within a galaxy rather than between galaxies in a cluster, with the exception of this lowest redshift pair of complexes. The distribution of velocity separations for the heavy element systems given in Table 2 is shown in Figure 8.

5. CONCLUSIONS

The high-resolution spectra of Q1100−264 in the Lyα forest region have revealed that:

1. The Lyα forest lines have a wide range of Doppler parameters, and there are no cases where the inferred cloud temperatures must be less than 10^4 K. This absence of systems with low Doppler widths contrasts with the results obtained by Pettini et al. (1990) for a sight line towards 2206−199. We have

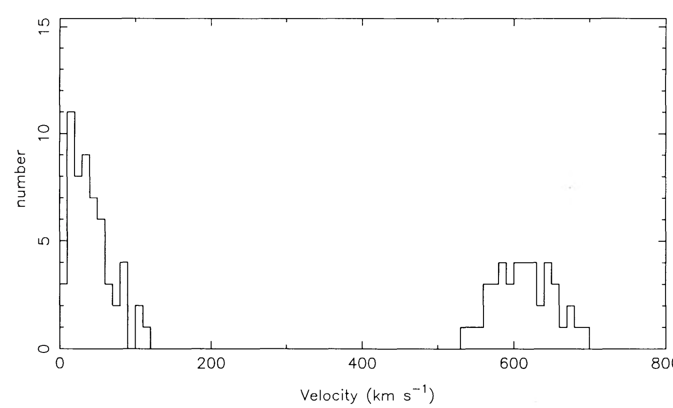

FIG. 8.—Velocity separation distribution for the heavy element systems. The peak at 600 km s^{-1} is due to the presence of multiple Mg II doublets at $z = 0.356$ and 0.359.

no plausible explanation for these differences, and do not know which of the two sight lines is typical.

2. There is little evidence for a correlation between Doppler parameter and H I column density for the Lyα systems. Such a trend is evident if we select only those systems with small errors in the measured quantities, but this arises because the largest errors are associated with high Doppler width, low column density systems.

3. Complex velocity structure in three of the known heavy element systems, and in none of the six heavy element systems for which lines fall in the observed wavelength region is only a single component found.

We wish to thank the AAO mountain staff for their usual excellent support during the observing run, Andrew Cooke for clarifying some points concerning the estimation of errors, and Max Pettini for extensive discussions of the results.

REFERENCES

Atwood, B., Baldwin, J. A., & Carswell, R. F. 1985, ApJ, 292, 58
Baron, E., Carswell, R. F., Hogan, C. J., & Weymann, R. J. 1989, ApJ, 337, 609
Bergeron, J., & Petitjean, P. 1990, A&A, in press
Carswell, R. F., Morton, D. C., Smith, M. G., Stockton, A. N., Turnshek, D. A., & Weymann, R. J. 1984, ApJ, 278, 486
Carswell, R. F., Whelan, J. A. J., Smith, M. G., Boksenberg, A., & Tytler, D. 1982, MNRAS, 198, 91
Chaffee, F. H., Jr., Foltz, C. B., Bechtold, J., & Weymann, R. J. 1986, ApJ, 301, 116
Chaffee, F. H., Jr., Weymann, R. J., Latham, D. W., & Strittmatter, P. A. 1983, ApJ, 267, 12
Ferland, G. J. 1989, Ohio State University Astronomy Department Internal Report 89-001
Morton, D. C. 1975, ApJ, 197, 85
———. 1978, ApJ, 222, 863
Morton, D. C., York, D. G., & Jenkins, E. B. 1988, ApJS, 68, 449
Petitjean, P., & Bergeron, J. 1990, A&A, 231, 309
Pettini, M., Hunstead, R. W., Smith, L. J., & Mar, D. P. 1990, MNRAS, 246, 545
Robertson, J. G. 1986, PASP, 98, 1220
Steigman, G., Strittmatter, P. A., & Williams, R. E. 1975, ApJ, 198, 575
Walker, D. D., & Diego, F. 1985, MNRAS, 217, 355
Walker, D. D., Diego, F., Charalambous, A., Hirst, C. J., & Fish, A. C. 1986, Instrumentation in Astronomy VI, Proc. SPIE, 627, 291